Thermal cycling test of solid particles to be used in concentrating solar power plants

Alejandro Calderón[1], Camila Barreneche[1], A. Inés Fernández[1] and Mercè Segarra[1*]

[1]DIOPMA, Department of Materials Science and Physical Chemistry, Universitat de Barcelona, Martí i Franquès 1, Barcelona 08028, Spain.

ABSTRACT

Durability and reliability of solid particles to be used in concentrating solar power tower plants is crucial for the project viability. Solid particles materials to be implemented in concentrating solar power plants are thermal aged and thermal cycled in this study to evaluation of solid particles at high temperatures. A homemade device has been developed to perform accelerated-durability tests, that allows emulation of thermal cycling stress from days to years, and even evaluate the 11,000 cycles expected to be reached during 20 years' plant's lifetime in less than four months. A detailed description of the operation of this device is included in this paper. In addition, current solar absorptance, chemical composition, physical properties, thermal characteristics, and morphologic analysis of the samples before and after thermal treatments have been performed. The materials under the study are the most reliable solid particles reported in CSP field: silicon carbide (SiC) and CarboHSP® 30/60. Characterization results show that SiC is more affected on its durability by thermal cycling than by constant temperature aging treatment while CarboHSP® is affected by temperature aging rather than thermal cycling. SiC reacts with oxygen to form SiO_2 on the surface, with a positive effect in its solar absorptance. Nevertheless, with thermal cycles, SiC particle surface becomes damaged and the reaction continues with more new exposed surface. Meanwhile, CarboHSP® reduces its solar absorptance with high temperature only due to changes in its surface chemical composition. However, thermal cycling shows no negative effect in CarboHSP® properties.

Keywords: solid particles; thermal energy storage; concentrated solar power; solar tower; heat transfer fluid; accelerated thermal cycling

1. INTRODUCTION

It is expected that, with the appropriate support, Concentrating Solar Power (CSP) technology can reach over 11% of global electricity generation by 2050 [1,2]. Just in 2017, 11 TWh were produced by CSP compared to 1 TWh in 2000. This capacity is estimated to reach 68,000 MW of power in 2040, reflecting a big increase of two orders of magnitude compared to the 4,650 MW registered in 2015, and the 1,250 MW power capacity installed in 2010 [3,4].

CSP with central tower configuration is a promising option for harvesting solar power due to the high power that can be reached, with a high thermal-to-electric conversion efficiency (due to the high working temperature), high land efficiency, and large scale thermal energy storage [1,5].

CSP plants offer, within its design, energy storage with high efficiency. This fact gives to CSP an advantage over other clean energies like photovoltaic or wind, since it can produce electricity at any time after sunset and for at least 8 hours [6,7].

For the International Energy Agency (IEA), CSP is considered favorable for those regions with high direct normal irradiance (DNI) such as North Africa, southern Africa, the Middle East, northwestern India, the southwestern of the United States, Mexico, Peru, Chile, the western part of China and Australia. However, other regions with less favorable DNI like the south of Europe, Turkey, southern United States, central Asian countries, places in Brazil and Argentina, and some other parts of China, are also viable for CSP implementation [1].

The current state-of-the-art of the technology shows that the best commercial configuration for CSP towers is the one that uses molten salts as both thermal energy storage (TES) and heat transfer fluid (HTF) [8]. Molten salts working on CSP plants can reach over 500ºC, and they show technological and financial viability. The salt known as solar salt (60% $NaNO_3$ + 40% KNO_3) is the main system used as TES material in commercial CSP plants [8]. For this kind of power plants, thermal-to-electric conversion is achieved with efficiency up to 40% [9,10]. Nevertheless, efficiency can be improved up to 50-60% by increasing the operation temperature. This is achieved by using more efficient thermodynamic cycles in which, theoretically, 80% conversion efficiency can be achieved by using cogeneration. However, molten salts become chemically unstable and highly corrosive at temperatures over 565 ºC [11–13]. To overcome this temperature limitation, solid particles have been proposed as TES since they can reach temperatures up to 1000 ºC without becoming chemically unstable or corrosive. Also, solid particles can easily fluidize and therefore can be used as HTF [14].

Current proposed solid particle CSP plant configuration is shown in Figure 1. This figure represents the configuration proposed by Sandia National Laboratories research team, with an open falling particle receiver, thermal energy storage in the tower and with moving bed heat exchanger (HEX) below the hot storage bin. Different configurations for solid particle CSP have been previously reported [15–17]. Despite similarity to current molten salts tower configuration, the transport, heat exchange, storage silos and receiver should be designed or adapted for handling granular materials around 1mm or smaller [15]. There are very active research topics for the overall plant design, especially for the solar receiver [18]. However, optimal solid particle materials must be screened and properly evaluated to decide the final material selection.

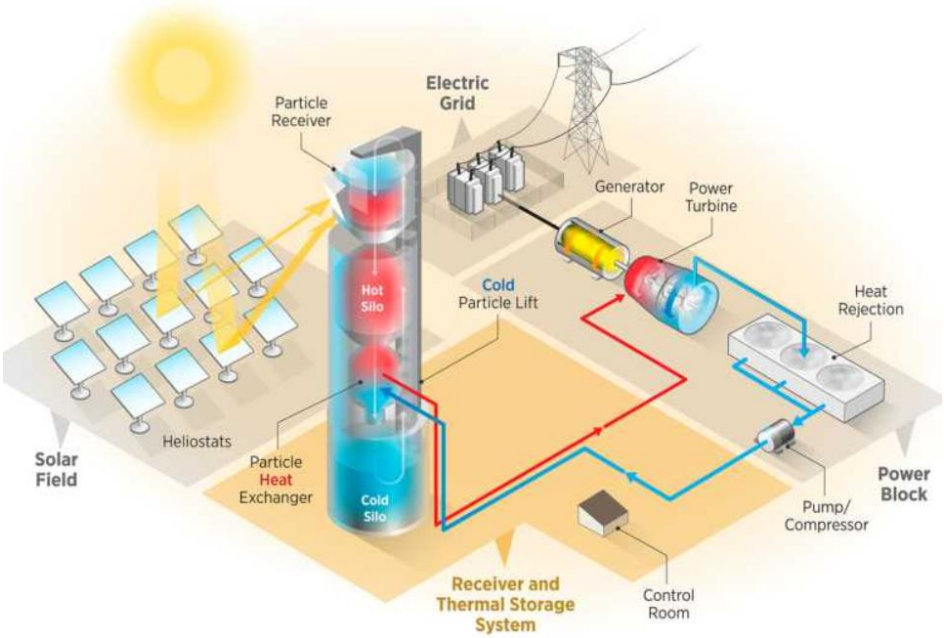

Figure 1. CSP solid particle system with TES and falling particle receiver [16]**.**

There is a lack in the literature regarding the mechanisms that solid particle will follow when they are used and applied in this kind of concentrated solar power plants. However, several changes can be found when the particles are under thermal treatments. The particles can change their geometry, by losing size, roundness or sphericity [19]. Moreover, the thermal treatments can change the specific heat or the solar absorptance due the chemical changes, e.g. solid particles oxidation [20,21]. Therefore, particle media durability is essential for a proper material selection. This is affected by thermal and mechanical combined stresses. Wear (mechanical interaction between the solid particles and the system materials) and attrition (mechanical interaction between the solid particles themselves) are the interactions that determine

the mechanical stresses [22]. Thermal stability is related to the high temperature exposure for long periods when particles are stored. Moreover, it is related to thousands of thermal heating-cooling cycles between low and high temperatures performed during power plant lifetime [23]. In the present study, thermal aging and accelerated thermal cycling analysis have been carried out in order to perform accelerated-durability tests for solid particles (SiC and Carbo HSP®) and relate the main results with the reliability of these solid particles in CSP tower plants.

2. MATERIALS and METHODOLOGY

2.1. Materials

Two materials were selected based on the materials reported in the existing bibliography, considering the properties listed in Table 1.

These selected materials were thermally aged and thermally cycled (as described in Section 2.2), and evaluated by different characterization techniques for studying their durability and reliability. The materials under study are Carbo HSP® [24] from CARBO Ceramics Inc., and black silicon carbide (SiC) [25] from Panadyne Inc., which have been suggested by several authors as excellent candidate materials for solid particle CSP [11,24–29].

Carbo HSP® is a synthetic proppant originally designed for hydraulic fracture industry, while SiC is a highly thermal shock and corrosion resistant material commonly used for seal faces, bearings, turbine rotors, pistons, hydraulic plungers, cylinder liners, aircraft armor, as reinforcements in ceramic and metal matrix composites, etc. [30].

Table 1. Reported properties of SiC and Carbo HSP ®

Property	Silicon Carbide				Carbo HSP®		
Melting point (°C)	2150 – 2250 [30]				2000 – 2100 [31]		
Service temperature (°C)	1470 – 1540 [30]				1500 [31]		
Thermal conductivity (λ) (W/m·K)	0.90 – 1.10 * [30]				2 ** [27]		
Specific heat (C_p) (J/kg·K)	663 – 677 (at 400 ºC) [30]				1275 (at 700 ºC) [28]		
Composition	Min 99.3% SiC	Max 0.4% SiO_2	Max 0.02% Magnetic Iron	[32]	83% - Al_2O_3	5% - SiO_2	[28]
	Max 0.4% C	Max 0.2% Si			4% - TiO_2	7% - Fe_2O_3	
Absorptance (α)	N/A				0.934 [24,28]		
Emissivity (ε)	0.83 - 0.96 [33]				0.843 [24]		
Cost (€/kg)	13 – 18.6 [30]				0.50 – 0.92 [34]		

ρ (kg/m³)	intrinsic: 3000 – 3200 [30], bulk: 1290 – 1570 [32]	intrinsic: 3560 [27], bulk: 2000 [28]

* Thermal conductivity for intrinsic material, ** Thermal conductivity of particle bed.

N/A: not available.

2.2. Thermal treatments

The temperature effect produced on the studied solid particles has been evaluated in this study by applying two different tests. Samples have been characterized before, after each thermal treatment, and at intermediate states.

Test 1: thermal aging test

Thermal aging is defined as the degradation of a material over time, due to its exposure to temperature. This test was performed by placing the studied samples in a sintered alumina crucible into a laboratory furnace. Temperature has been set at 900ºC and samples were kept at this temperature for 500 hours. Even though the most significant changes were expected during the first hours, the long-term stability of the material was primarily evaluated with this test.

Test 2: thermal cycling test

To evaluate the thermal aging due to thermal cycles a novel automatic cycling device was designed for this specific purpose. No device like this has been found either commercially or at the research level. Each thermal cycle was performed between 300°C and 900°C. During the process, the materials were in contact with air and without any pressure control, since these are the boundary conditions at the CSP power plant. Air contact was assured since one end of the tube was open during the tests, and an airflow test was performed through the packed particle media before starting the thermal cycling. The evaluated materials were thermally aged during 500 hours at constant 900 ºC before thermal cycling. This developed device is described in the next section.

2.3. Experimental set-up: Thermal cycler device

To test the thermal cycling durability of solid particles a device has been developed by University of Barcelona researchers. This setup can perform, in three months, a test equivalent to a daily cycle for 30 years between the established temperature limits. Each thermal cycle takes between 11 (for black silicon carbide) and 14 minutes (for Carbo HSP®) for the temperature range between 300 ºC and 900 ºC, depending on the material being cycled. Each thermal cycle includes both thermal charging and discharging,

meaning that a cycle starts at 300 °C and ends when the particles get 300 °C again. No reference has been found about the time needed for the particles to remain in the receiver (charging) or in the heat exchanger (discharging), as theoretical time calculations have shown to differ significantly from those of the pilot scale (when the design has been tested) [27,36–38]. For that reason, cycling tests have been designed to be as short as possible, although the time for each cycle is finally defined by the tested material.

The temperature range was determined according to the ideal conditions of the CO_2 super critical Brayton thermal-to-electric cycle, in which conversion efficiency can reach up to 60% under these conditions [39]. This conversion cycle has been proposed by Sandia National Laboratories for moving packed-bed heat exchanger [38].

The device (see Figure 2) consists of two furnaces: one at the highest temperature (below) and the other at room temperature (above). Both furnaces have holes on top, and the one at room temperature has also a hole below so the alumina tube can move across one to the other (Figures 2b and 2c).

The granular material sample is placed inside the sintered alumina tube and this tube is automatically moved between the two furnaces. The temperatures inside the furnaces are controlled: the hot furnace at 1050 °C and the cold furnace at room temperature (~23 °C). The upper part of the tube is painted in black and a color sensor helps to identify the position of the tube in the device.

To move the tube automatically for 24 hours a day and unattended, several system components were added as shown in Figure 3. A motion unit is responsible of moving the tube between the two furnaces. The sample remains at the heating position (Figure 2c) until reaching 900°C. Afterwards, the tube is automatically moved to the cooling position (Figure 2b) until the sample reaches 300°C, at which time it moves back down to the heating position, thus completing one thermal cycle, and starts again.

Temperature is monitored and controlled by four Type K thermocouples: one inside the tube for monitoring the temperature of the sample, one in each furnace, and the fourth in the motion unit for its thermal monitoring. The temperature sensor inside the tube, which was in contact with the sample, was carefully placed in the center of the volume occupied by the particles. This guarantees that the lowest and highest temperatures are reached by all the material. In addition, the inner diameter of the tube was 14.5 mm, which resulted in less than 7.25 mm in width of material between the thermocouple and the alumina tube (whose thickness was 2.75 mm).

To quickly cool the sample, an air fan was placed in the low temperature furnace, causing forced air convection on the outside of the tube when the sample is at the cooling position. This cooling unit uses ambient temperature air and it allows to enter low-temperature air to the furnace from the outside by refrigerating it. In addition, another air fan helps to prevent temperature increase at the motion unit due to natural convection of heat. For the same reason, a thermal gap has been left between the low temperature furnace and the motion unit.

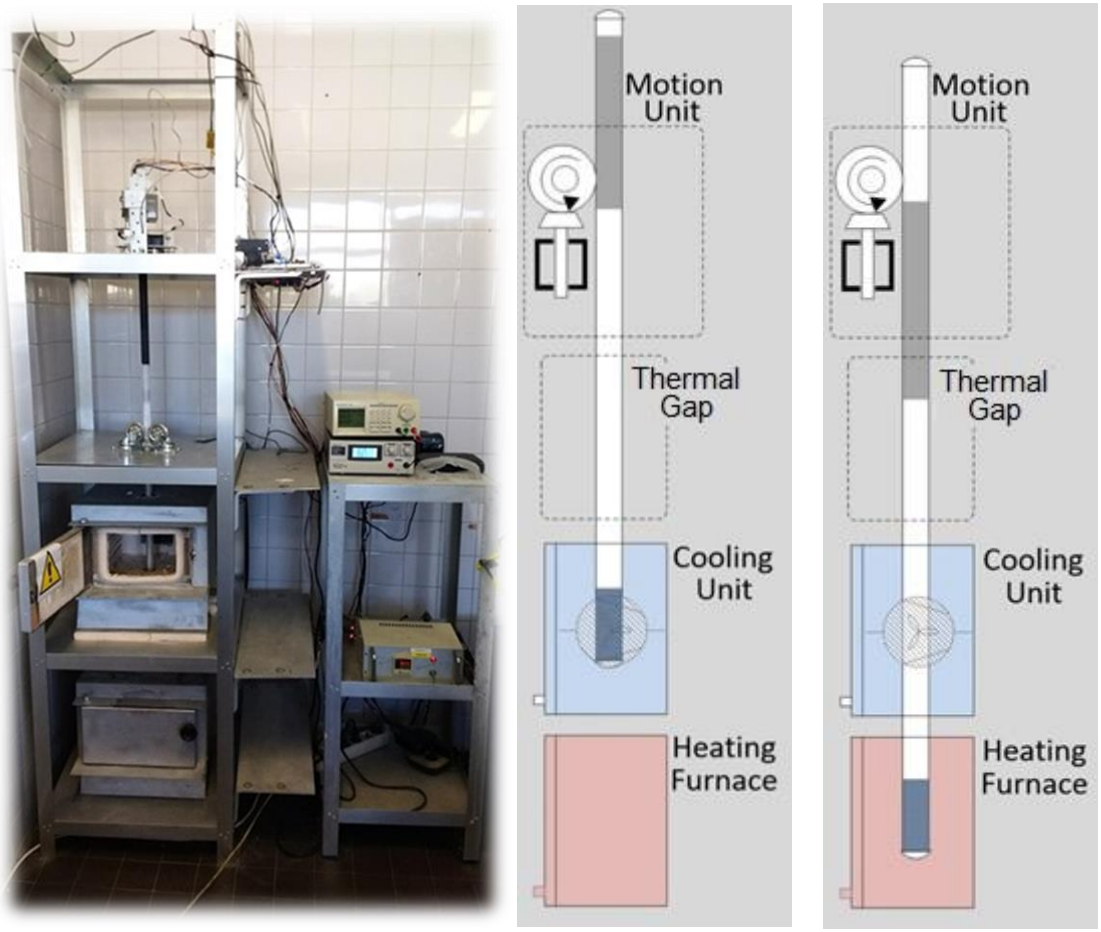

a) b) c)

Figure 2. a) Thermal cycling device; b) Scheme of the thermal cycling device at cooling position; c) Scheme of the thermal cycling device at heating position.

Since the device works unattended 24 hours a day, the controller monitors several safety conditions: it can interrupt the cycling process by turning off the power supply of both the heating furnace and the motion unit in case of alarm, while emiting an audible alarm sound.

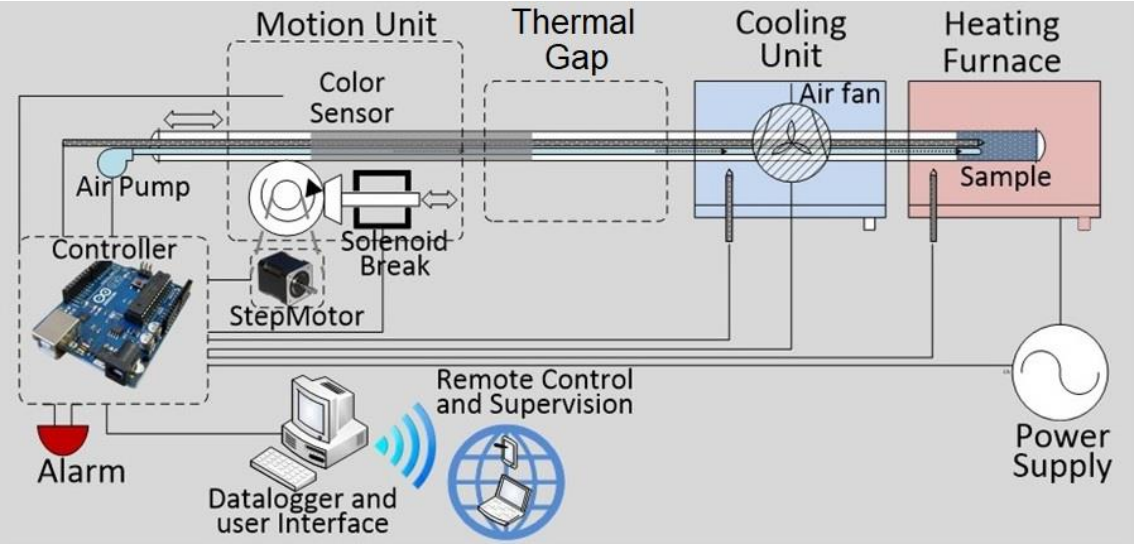

Figure 3. Thermal cycling device schematic layout.

The controller unit was built using an Arduino Mega 2560® card and an electronic board for all the electronic interfaces. This controller was programmed to handle the thermal cycles and the security triggers, as well as to communicate with the computer interface. For data collection and user control, a computer interface was developed as shown in Figure 4. This program receives all the data from the thermocouple, displays the recorded temperatures for the last hour on a graph, and stores all the data on a database for further analysis (if needed). Also, the basic functions and parameters of the device can be managed, such as starting/stopping the thermal cycles, defining the number of cycles to be performed, the set point for low and high temperatures, the alarm tolerance temperature, activating the alarm, etc.

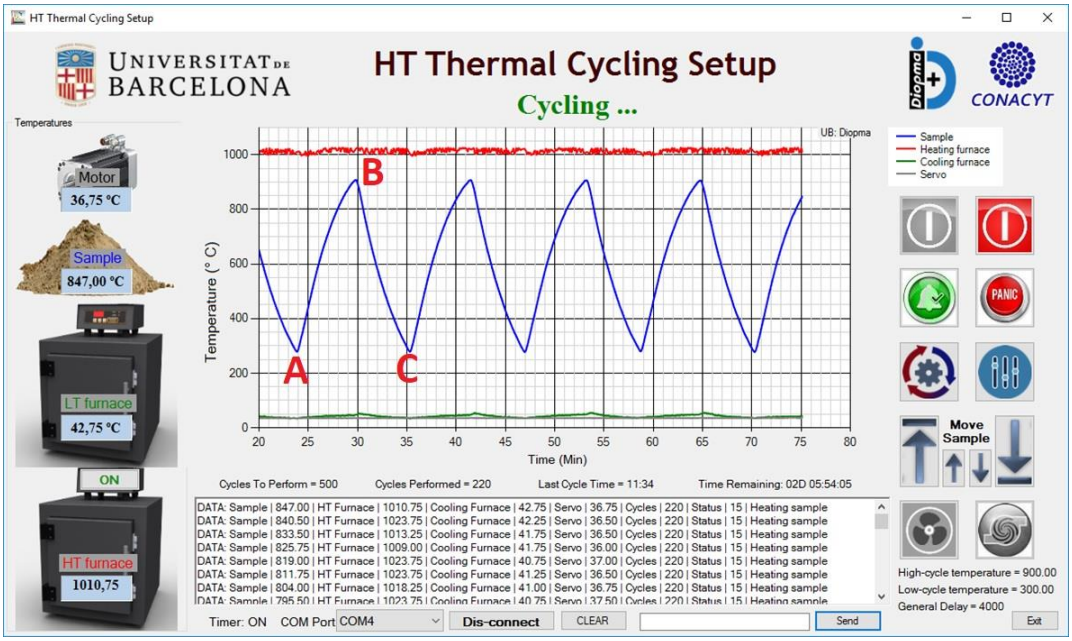

Figure 4. Thermal cycling device computer interface

Figure 4 shows a typical temperature profile obtained for a sample under thermal cycling. On the left you can see the temperature of the motor, the sample and the two furnaces. Point A corresponds to the sample in the cooling position, point B when it has reached the maximum temperature, and point C when it returns to 300 °C. The time elapsed between A and B, and between B and C depends on the thermal diffusivity of the sample tested. Thus, the greater the energy density (that is the product of density by the specific heat) of the material, and the lower the thermal conductivity, the more time it will take to reach point B and further re-cool (reaching point C).

2.4. Characterization

Both selected materials were thermally treated (with thermal aging and thermal cycling tests) and characterized by Scanning Electron Microscope (SEM), Particle Size Distribution (PSD), Energy Dispersive X-ray Spectroscopy (EDS), X-ray diffraction (XRD), density by Helium pycnometer, Thermo-Gravimetrical Analysis (TGA), Differential Scanning Calorimetry, and by solar absorptance spectrophotometer analysis. Analyses were performed to the samples progressively, beginning with the materials as received, then after thermal aging, and finally after thermal cycling; this allowed to analyze the effect of each of the thermal stress applied to sample durability. Notice that all the samples under study are completely dried when are characterized since they were previously thermal treated. The samples characterized as received also have been dried at 105 ºC for 24 hours. Therefore, the humidity does not affect to any results in the full characterization performed.

Physical and morphological characterization.

- Helium pycnometer measures the real density of the samples. The real density measurements were carried out in a Micrometrics Pycnometer Accu-Pyc 1330. The differences between samples before and after thermal tests can be due to sinterization of materials or particle breakage. These morphological changes can result in significant real density changes.
- Particle size distribution of the samples was measured with a Beckman Coulter LSTM 13 320 laser diffraction particle size analyzer with Universal Liquid Module using Electrical Sensing Zone Method for Particle size distribution (PSD) analyses. Data used for analysis was the average of three measures made for each sample. Particles were scattered using water for avoiding particle agglomeration. Results were analyzed using Fraunhofer mathematical model, which is used for opaque

materials and bigger than 30 µm. The differences between samples before and after thermal treatments can be attributed to sinterization or particle breakage.

- Scanning electron microscopy (SEM) was performed in a FEI Quanta 200 SEM. The images can show changes in the morphology of the samples before and after the thermal treatments, as well as cracks on the solid particles surface.

Chemical characterization.

- Energy Dispersive Spectroscopy (EDS) was performed in a FEI Quanta 200 SEM integrated with EDS detector, obtaining semi-quantitative results between 0 and 11 keV, performed on single spots with an exposition time of 100 seconds. All samples were coated with graphite for electric conductivity requirement.
- X-ray diffraction (XRD) analysis was performed in an XRD from Philips MRD to identify the crystalline phases in the solid particles. Any significant changes in the chemical composition leading to a structural modification after thermal treatments may be detected.

Optical properties characterization.

- In order to analyze the capacity of the SiC and Carbo HSP® particles to absorb solar radiation, a Perkin Elmer Lambda 950 spectrophotometer with a 150 mm integrating sphere was used to measure the bluk particle properties of the materials under study. Absorptance was measured each 20nm within a 300nm to 2500nm wavelength range using 1-inch diameter circular sample. Once absorptance was obtained for each wavelength, a trapezoidal integration was performed and weighted with respect to solar spectrum AM 1.5 in order to obtain the solar absorptance value for the whole 300nm to 2500nm wavelength range. For absorptance measuring of granular materials a previous developed technique was used employing a special crucible [20].

Thermal characterization.

- The thermal energy storage capacity of both solid particle materials was studied by differential scanning calorimetry (DSC) technique. The method used was the areas method reported by Ferrer et al. [40] to characterize TES materials. The analyses were run in a DSC 822 from Mettler Toledo at 500 °C. Around 7 mg samples were

studied and 50 mL/min N_2 flow was applied. Three different subsamples were measured for each sample (before and after thermal treatments).

- Material evaluation with thermogravimetrical analysis (TGA) was made for the material as received, after aging at 900ºC, and after thermal cycling as the worst scenario. The measurements were conducted between 300ºC and 900ºC under N_2 atmosphere, with a flow of 80 mL/min, at a heating rate of 10 K/min, with around 30 mg mass, in a TA Instruments SDT Q600. The TGA results will corroborate that the samples do not contain water (as molecules absorbed or as humidity) in their composition and any other decomposition process.

3. Results

3.1. Physical and morphological characterization.

Real density

Real density changes measured by Helium pycnometer for each material (Carbo HSP® and SiC) after thermal treatments are presented in Table 2. Carbo HSP® shows no significant variation, while SiC shows a slight decrease of around one percent after the thermal cycling test. This change reflects that a change in SiC particles took place and are in concordance with EDS results where slight chemical composition changes were seen in the SiC case.

Table 2: Real density (kg/m^3) for SiC and Carbo HSP® as received and after thermal treatments.

Material	As received	After 500 hours aging	After 1500 cycles
Carbo HSP®	3645.1 ± 0.5	3635.5 ±0.2	3637.4 ±0.2
SiC	3206.4 ±0.5	3202.4 ±0.5	3176.5 ±0.1

Particle Size distribution (PSD)

Evolution of PSD with thermal treatments for Carbo HSP® and SiC are shown in Figure 5a) and Figure 5b), respectively. Carbo HSP® shows a very similar profile and mean values for volume and number distributions showing that the Carbo HSP particles

have a very homogeneous size. A slight displacement is observed related to a small increase in mean particle size due to thermal treatments. Meanwhile, SiC PSD seems to be more affected by thermal shock than by aging. Although the volumetric distribution slightly changes for the thermally cycled sample, the number distribution shows an increase in the fraction corresponding to smaller particles, between 90 µm and 150 µm, thus reflecting that there has been an increase of fines probably originated by the fracture of the bigger particles due to thermal cycles. In addition, the impact of particle roundness on the stability of the oxide layer on the SiC particles has also importance, and this term is difficult to measure by PSD.

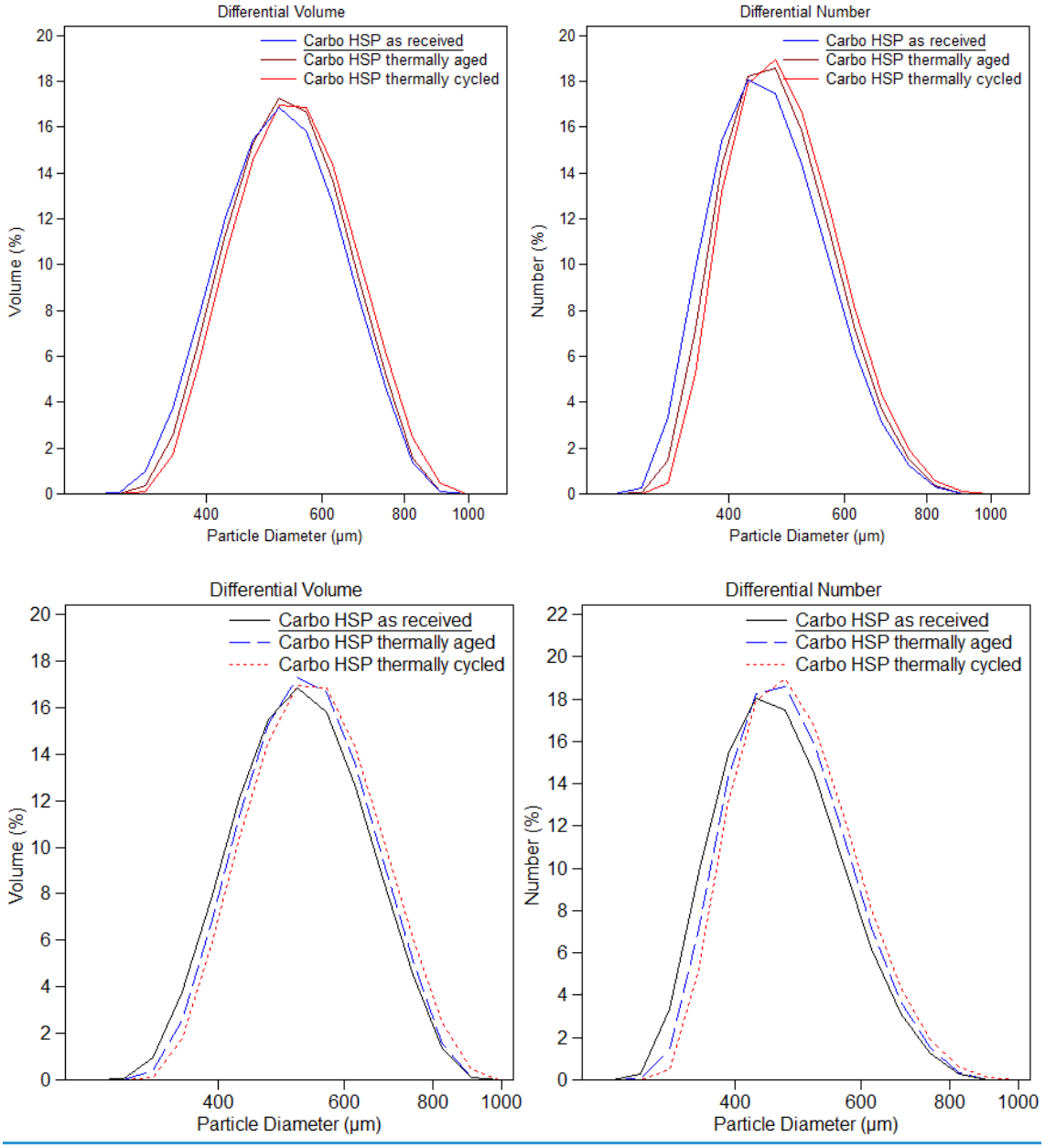

a)

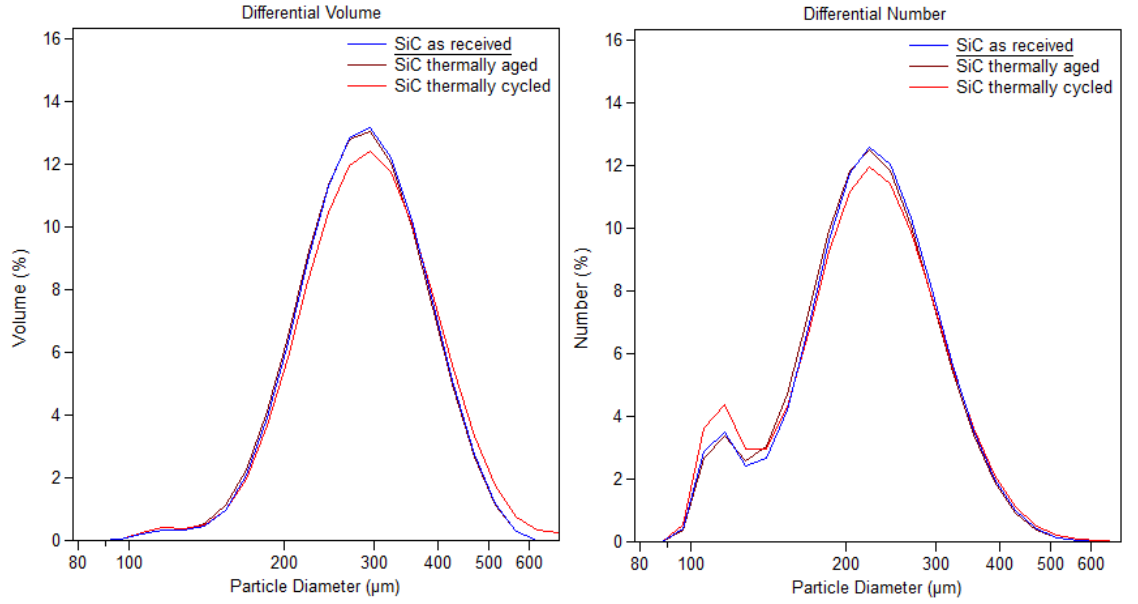

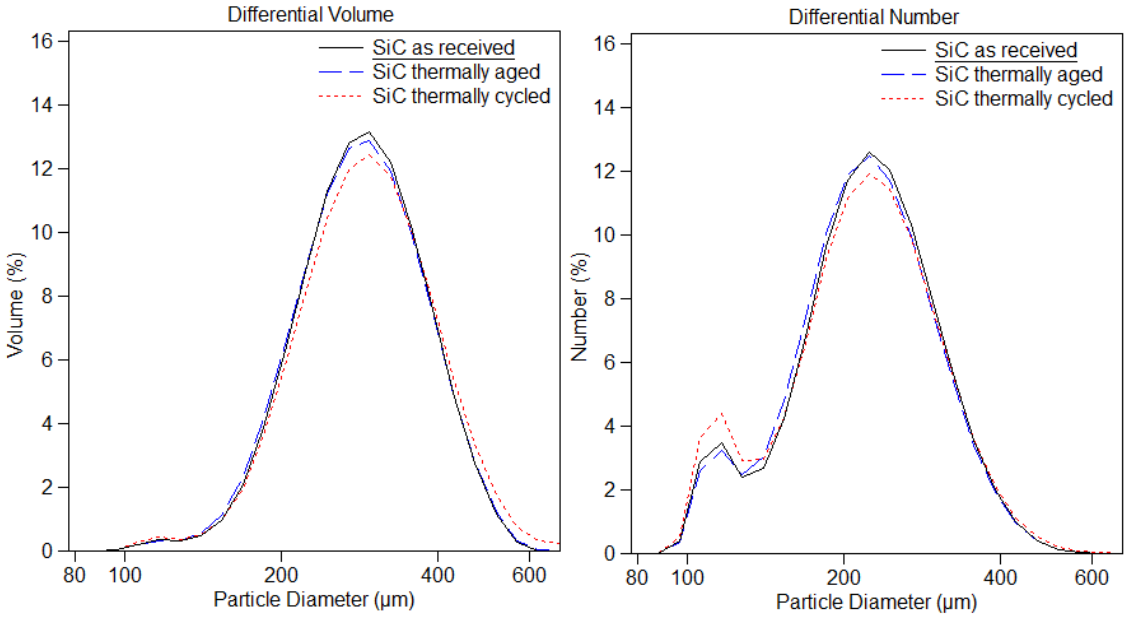

b)

Figure 5a) PSD for Carbo HSP® samples; b) PSD for SiC samples.

SEM analysis

SEM images of Carbo HSP® show that, apparently, particles were not affected by the thermal stress tests. This material is one of the most promising candidates to be used as solid particle materials for CSP since no changes can be observed on its surface as shown in Figures 6.a), 6.b) and 6.c). In the case of SiC, SEM images (Figure 6) show some changes on the surface of the particles, mainly after 1500 cycles between 300°C and 900°C. These changes can be clearly observed in Figure 6.f) where several cracks and fissures on the material surface appeared. Magnification of most significant material irregularities have been added for the three SiC samples.

EDS analysis

EDS semi-quantitative elemental analysis showed that there is non-detectable change in the surface composition of Carbo HSP® due to thermal treatments. EDS analysis for Carbo HSP® were performed in some areas free of defects or in small particles. For SiC, EDS shows a slight change since oxygen appears in thermally aged sample and in the thermally cycled sample (Figure 7). This suggests that SiC surface reacted with oxygen in the air during the test and formed SiO_2 while releasing CO_2. Carbon presence cannot be evaluated, since all Carbo HSP® and SiC samples were graphite-coated to increase electrical conductivity for SEM analysis. EDS analysis were performed on the most pronounced edges of the particles, since authors assume that the increase of exposed surface will result on elevated reactivity compared to the flat surface of the particles.

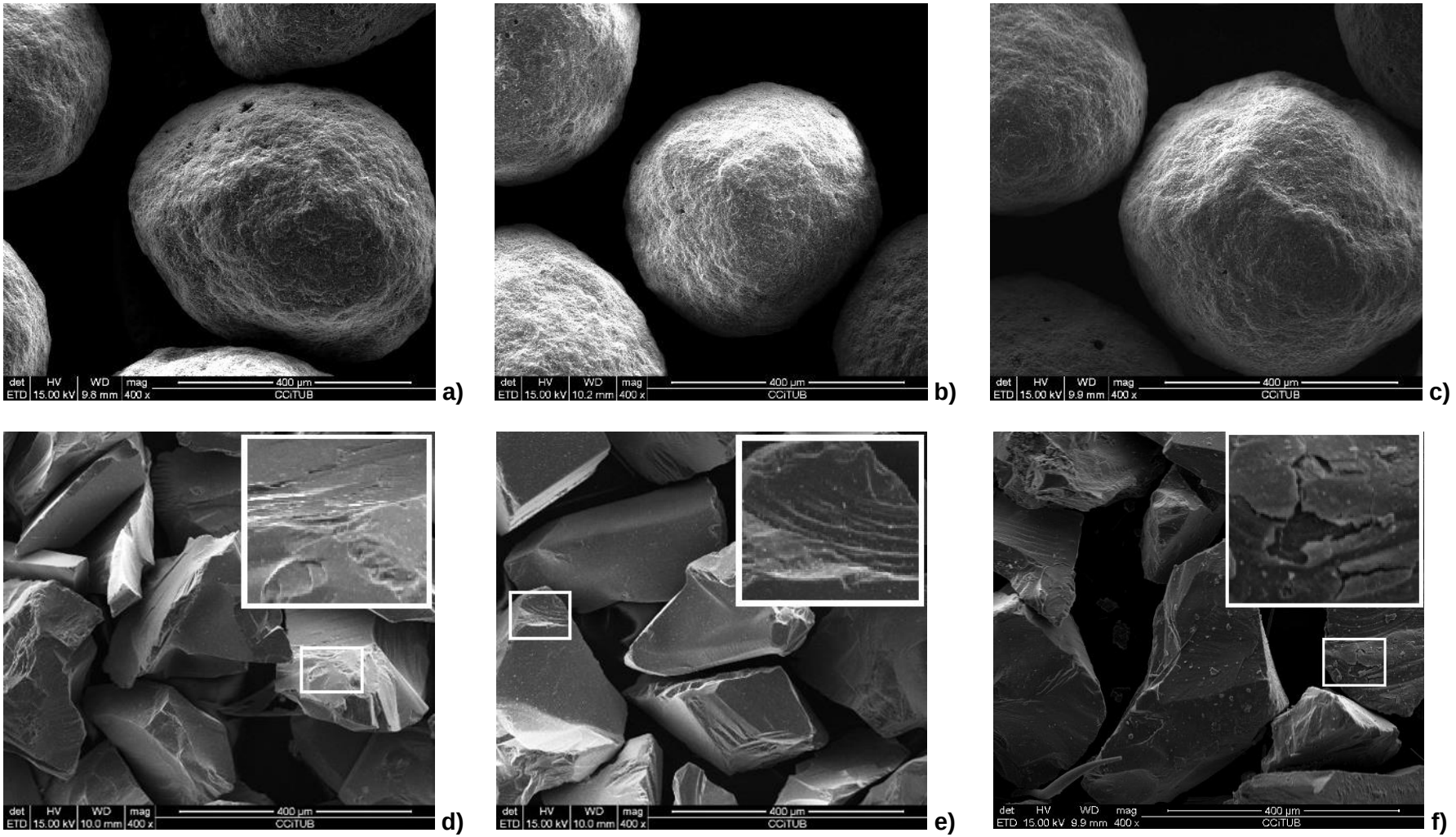

Figure 6. SEM images of Carbo HSP® sample a) as received; b) after 500 hours at 900 ºC; c) after 1500 thermal cycles between 300 ºC and 900 ºC. SEM images of SiC with inserted magnification d) as received; e) after 500 hours at 900 ºC; f) after 1500 thermal cycles between 300 ºC and 900 ºC

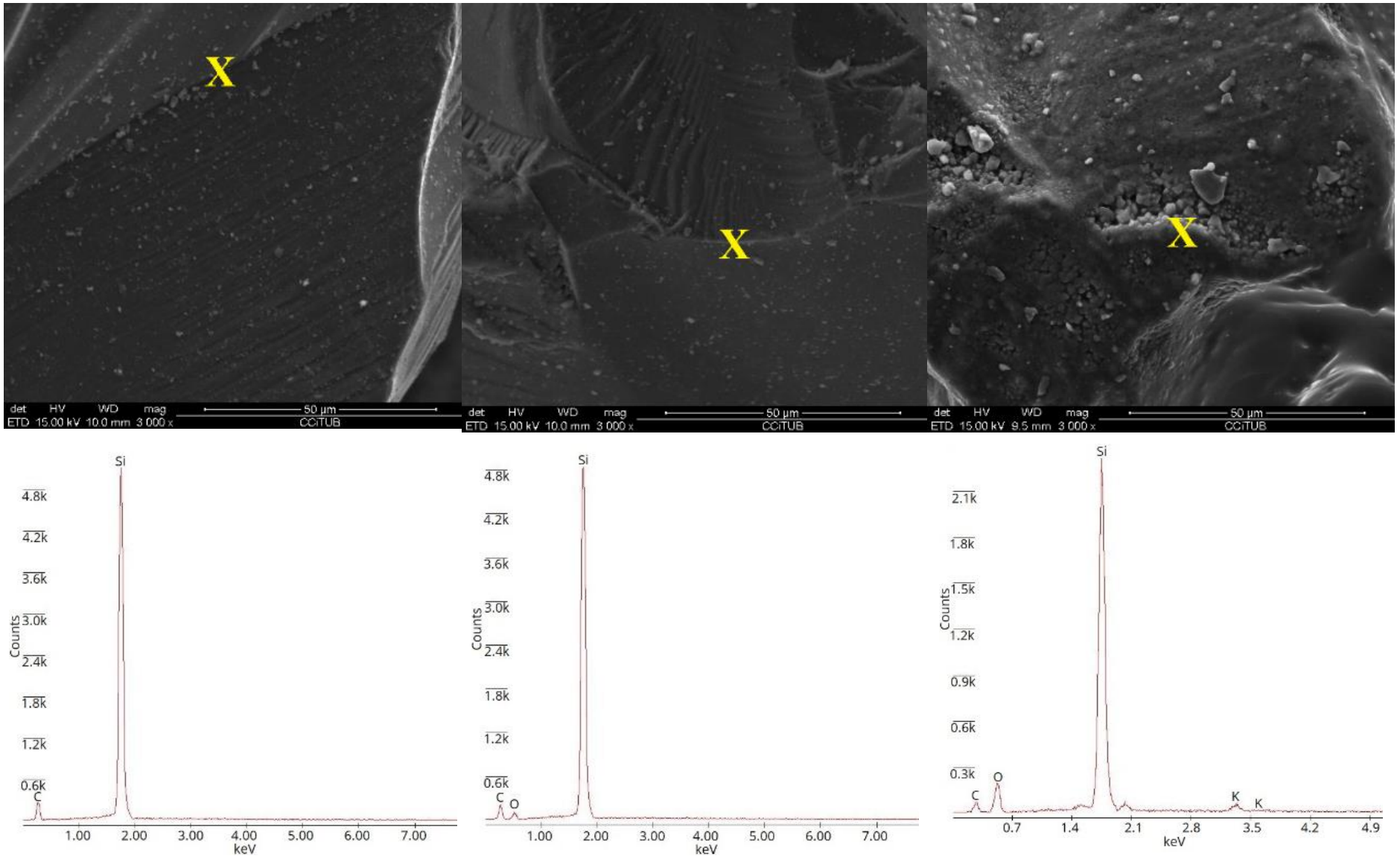

a) b) c)

Figure 7. SEM images and corresponding EDS analysis of SiC a) as received; b) thermally aged; c) thermally cycle

X-Ray diffraction analysis

XRD diffraction analysis of Carbo HSP® (Figure 8) shows that the main crystalline phases are Al_2O_3, SiO_2 and Fe_2O_3 with no visible composition changes after aging treatment and thermal cycling tests. Figure 7 represents the three Carbo HSP® samples, which present identical XRD spectra.

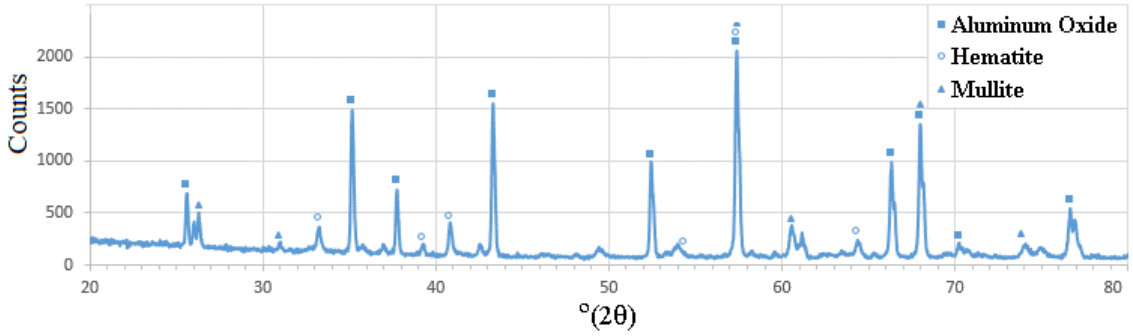

Figure 8. XRD spectra for Carbo HSP® for all studied conditions (as received, aged at 900 ºC for 500 hours, and after 1500 cycles between 300 ºC and 900 ºC).

For SiC, the presence of oxygen during thermal treatments could favor a reaction with SiC, releasing CO_2 and leaving SiO_2 on the particle surface. For original and aged samples only SiC was detected, since only fractions with more than 4% w/w can be securely identified. The change on SiC particles composition can be appreciated by XRD analysis. Figure 9a shows XRD analysis for a SiC samples as received, after 500 hours at 900 ºC, and after 1500 thermal cycles, which differs only in one peak (marked with a triangle). In Figure 9b analysis for the three samples are presented between 20º and 30º position in a logarithmic scale to appreciate the phase of SiO_2 that was detected in the cycled sample at about 22º position. Pure SiC sample should not react with oxygen at temperatures under 1200ºC. Nevertheless, there has been reported that the SiC develops a protective surface layer of SiO_2 which prevents SiC decomposition [41]. It is important to remember that the XRD analysis detects only crystalline structures of the material, whereas changes on amorphous fraction are not detectable. In this case, SiC base line indicates that it is almost in pure crystalline form.

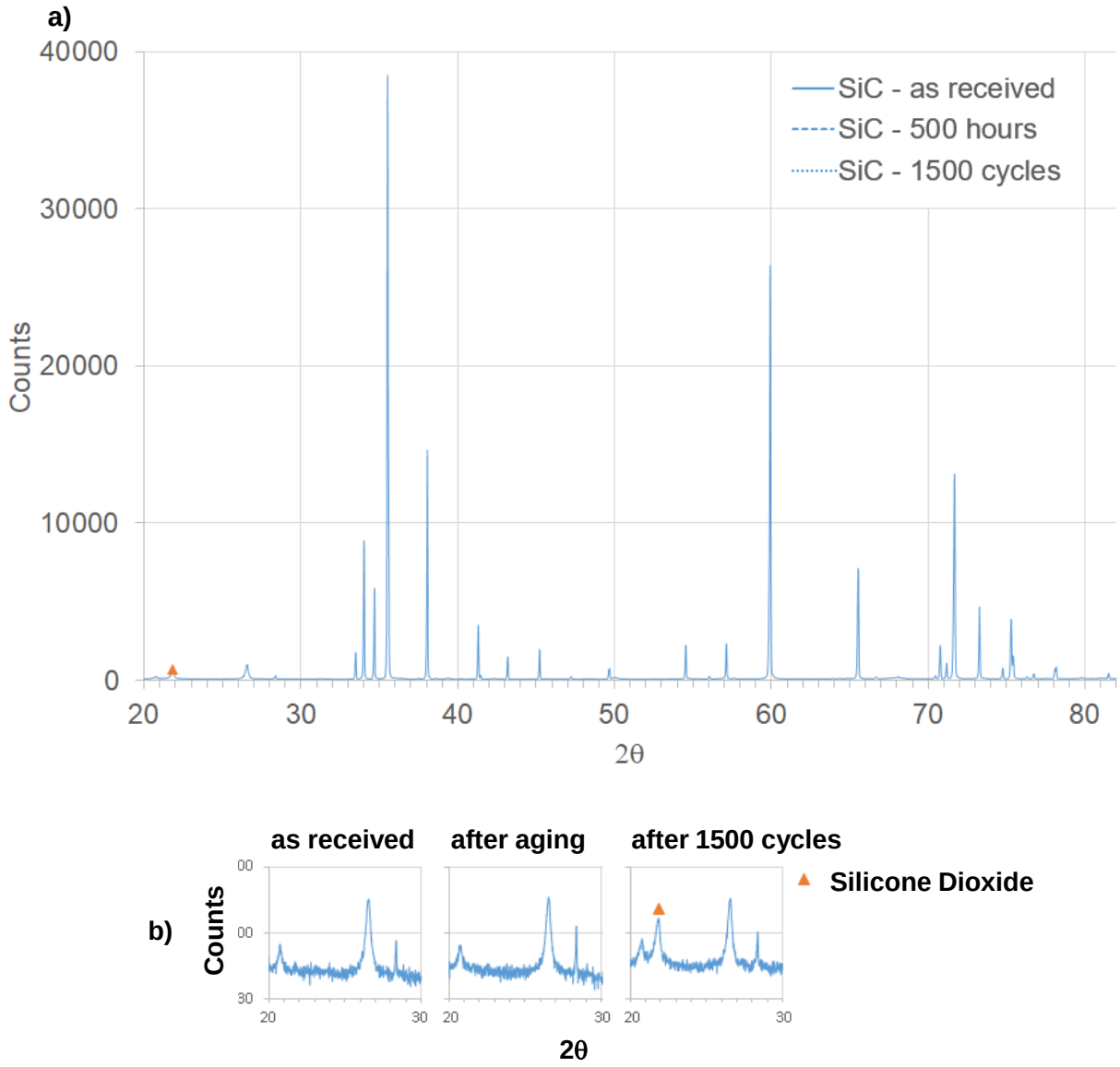

Figure 9. XRD spectra for SiC a) as receive, after aging at 900 ºC for 500 hours, and after 1500 cycles between 300 ºC and 900 ºC, b) expansion of the spectrum between 20 and 30º angle for as received, after aging at 900 ºC for 500 hours, and after 1500 cycles between 300 ºC and 900 ºC.

3.2. Optical properties characterization: Solar absorptance

Solar absorptance results of Carbo HSP® can be observed in Figure 10, where solar absorptance decay is observed after thermal aging (Figure 10a), while thermal cycling (Figure 10b) does not affect the sample on its solar absorptance capacity. Results show that for an early thermal aging stage the absorptance decreases constantly, but it is not severe enough compared to other proposed materials like silica sand, olivine, slate, alumina, etc. [20,21]. Therefore, it is advised to perform long thermal aging and thermal cycling tests to guarantee the material stability during the expected lifetime. For SiC, both thermal treatments had a positive effect on its solar

absorptance: even during thermal cycling, solar absorptance increase continued. Results for SiC are shown in Figure 10c) and Figure 10d). It appears that thermal aging and thermal cycling benefits the solar absorptance of the silicon carbide particles. This is due to the chemical composition changes produced by both thermal treatments performed in this study.

In addition, for the case of SiC, solar absorptance increases with both thermal treatments due to the chemical oxidation this materials is suffering as it is shown in SEM images. However, further thermal cycling test is required in order to understand where the solar absorptance will stop its increment.

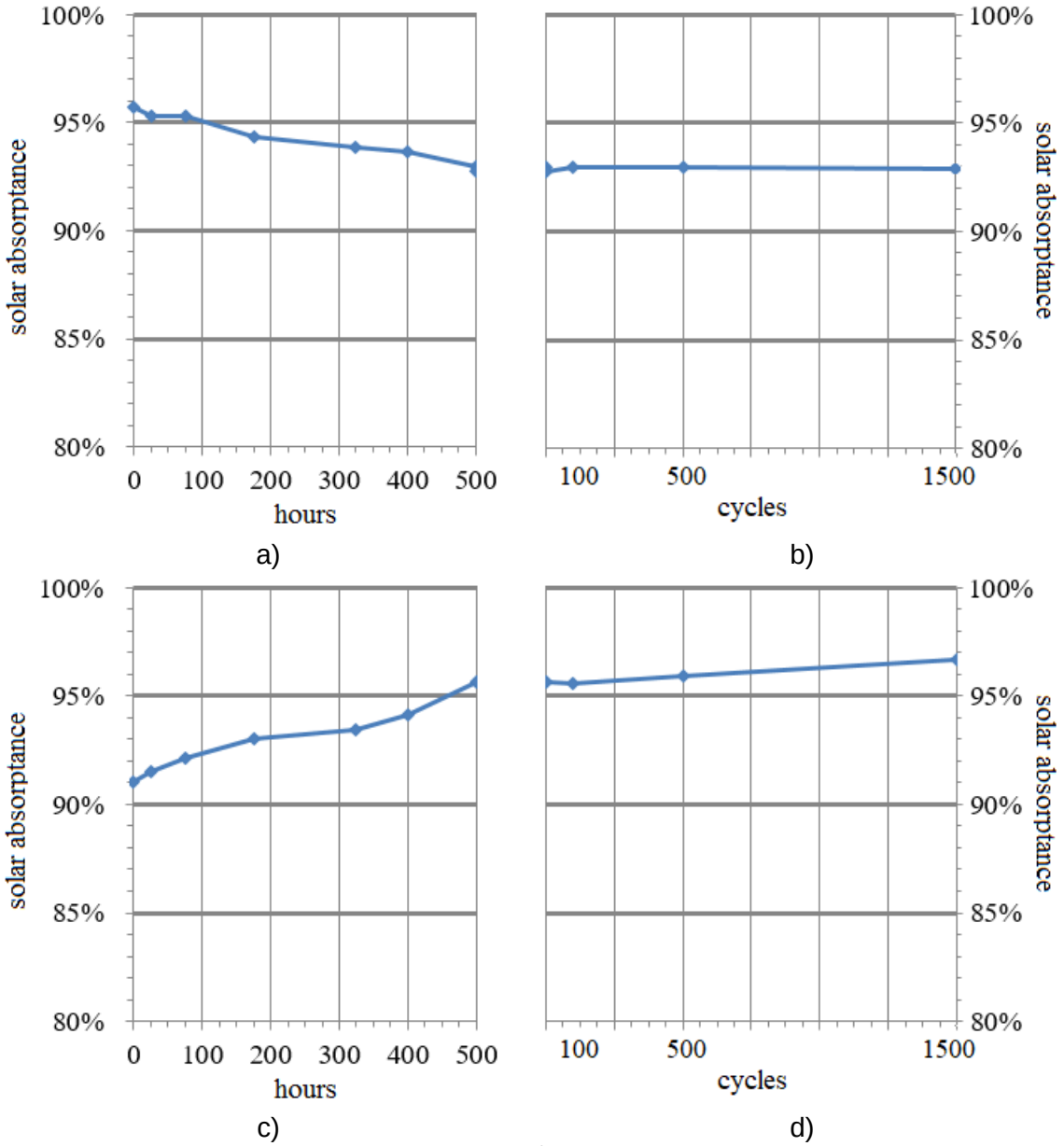

Figure 10.a) Solar absorptance of Carbo HSP® after thermal aging, and b) thermal cycling; c) solar absorptance of SiC after thermal aging, and d) thermal cycling.

On the other hand, for Carbo HSP, the results obtained are consistent with those one reported by Siegel et al. [39]: The absorptance of the Carbo HSP® after thermal aging slightly decreased. However, the thermal cycling does not affect to the absorptance and this is the first time this treatment is tested with these solid particles at very high temperature.

3.3. Thermal properties characterization: thermal storage performance

The thermal properties analyzed with the DSC in terms of specific heat (C_p) are listed in Table 3. The DSC measurements were performed at 500 ºC and three repetitions were run.

Table 3. Specific heat results (kJ/kg·K) for SiC and Carbo HSP® as received and after thermal treatments measured at 500 ºC.

Material	As received	After 500 hours aging	After 1500 cycles
Carbo HSP®	1.19 ± 0.01	1.14 ± 0.01	1.10 ± 0.01
SiC	1.31 ± 0.01	1.05 ± 0.01	1.00 ± 0.01

A reduction of the specific heat after thermal treatments is observed, being more significant in the case of SiC than for the Carbo HSP®, which is in accordance with the optical and chemical characterization and EDS results. In the case of Carbo HSP® the C_p reduction is around 7.5%.

However, the thermal treatments modified the SiC composition by oxidizing the SiC surface exposed to the environmental atmosphere. These chemical changes are shown in EDS results. The thermal energy storage capacity reduction measured in this study is significant, being around 20%.

TGA tests were performed up to 1250°C. Results for Carbo HSP® and SiC as received, thermal aged and thermal cycled showed that there was non-significant mass variation with temperature, within equipment measure limit of 1% of weight.

4. Conclusions and future work

In summary, the thermal aging tests reveal that this thermal treatment affects the material under study being more noticeable in the SiC case according to the C_p and XRD results. However, these chemical changes seem to benefit SiC solar absorptance. Moreover, the thermal cycling test performed in our own-developed equipment changes the chemical structure of SiC as shown in EDS results, being even more noticeable the SiC oxidation. This fact is confirmed by the C_p analyses, the XRD results, and can be appreciated in the SEM images obtained. Instruments

uncertainties are well known so only changes significantly above the instrument uncertainties have been considered.

Carbo HSP® after thermal aging and thermal cycling tests remains almost equal, thus being the material with highest reliability. Slight changes in its chemical structure causes a C_p slight decrease but this is neither appreciated in the XRD obtained results nor in the SEM images.

Results analysis has shown that black silicon carbide had major problems when dealing with long-term thermal cycling. Evidences have shown that the mean particle size lowers, and that the particle increases its reactivity with air. Particles damage can be observed by SEM, EDS and changes in the measured particle size. Previously reported SiO_2 surface layer protects the rest of SiC particle from reacting with oxygen present in air, but experimental evidence in this study has shown that thermal cycling causes thermal stress that breaks the SiO_2 coating, exposing new surface of SiC particle to oxygen. Carbo HSP® has higher resistance to thermal cycling and it is stable enough for longer thermal cycling evaluation, thus becoming a good candidate for CSP plants.

Thermal cycling evaluation has shown its relevance when selecting the best material available for this new type of CSP plants. Then, the novel thermal cycling device has shown to be effective to evaluate the thermal stress durability. Ensuring a proper and cheap material that can be used for all the power plant lifetime is essential for reaching a commercially viable system.

Future studies should include combined thermal and mechanical stress for a more accurate durability prediction studies. In addition, mechanical and thermal conditions should be similar to the ones in the solid particle CSP plant design.

Acknowledgements

This work was partially funded by the Ministerio de Economía y Competitividad de España RTI2018-093849-B-C32 (MINECO/FEDER). The authors would like to thank the Catalan Government for the quality accreditation given to their research group (DIOPMA 2017 SGR 0118). DIOPMA is certified agent TECNIO in the category of technology developers from the Government of Catalonia.

References

[1] International Energy Agency, Technology Roadmap - Concentrating Solar Power, (2010).

[2] International Energy Agency, Technology Roadmap - Solar Thermal Electricity, 2014.

[3] International Renewable Energy Agency, Renewable Capacity Statistics 2016, (2016).

[4] International Energy Agency, World Energy Outlook 2018, 2018.

[5] F. Trieb, C. Schillings, M. O'Sullivan, T. Pregger, C. Hoyer-Klick, Global Potential of Concentrating Solar Power, in: SolarPaces Conf. Berlin, SolarPaces Conference, Berlin, 2009.

[6] International Energy Agency, Technology Roadmap Energy Storage, (2014).

[7] C. Prieto, Advanced thermal energy storage research in demo plants for commercial systems, University of Lleida, Spain, 2016.

[8] K. Lovegrove, J. Pye, Fundamental principles of concentrating power (CSP) systems, in: Conc. Sol. Power Technol., Elsevier, 2012: pp. 16–67. https://doi.org/10.1533/9780857096173.1.16.

[9] C. Ho, High-Temperature Falling-Particle Receiver, U.S. Dep. Energy. (2012). http://energy.gov/sites/prod/files/2014/01/f6/55460.pdf (accessed January 26, 2015).

[10] M.T. Dunham, B. Iverson, High-Efficiency Thermodynamic Power Cycles for Concentrated Solar Power Systems, BYU Sch. 30 (2014) 758–770.

[11] C.K. Ho, B.D. Iverson, Review of high-temperature central receiver designs for concentrating solar power, Renew. Sustain. Energy Rev. 29 (2014) 835–846. https://doi.org/10.1016/j.rser.2013.08.099.

[12] K. Vignarooban, X. Xu, A. Arvay, K. Hsu, A.M. Kannan, Heat transfer fluids for concentrating solar power systems – A review, Appl. Energy. 146 (2015) 383–396. https://doi.org/10.1016/j.apenergy.2015.01.125.

[13] W.-D. Steinmann, Thermal energy storage systems for concentrating solar power (CSP) plants, Elsevier, 2012. https://doi.org/10.1533/9780857096173.2.362.

[14] Z. Ma, G.C. Glatzmaier, M. Mehos, Development of Solid Particle Thermal Energy Storage for Concentrating Solar Power Plants that Use Fluidized Bed Technology, Energy Procedia. 49 (2014) 898–907. https://doi.org/10.1016/j.egypro.2014.03.097.

[15] A. Calderón, A. Palacios, C. Barreneche, M. Segarra, C. Prieto, A. Rodriguez-Sanchez, A.I. Fernández, High temperature systems using solid particles as TES and HTF material: A review, Appl. Energy. 213 (2018) 100–111. https://doi.org/https://doi.org/10.1016/j.apenergy.2017.12.107.

[16] C.K. Ho, Technology Pathway - Particle Receivers, in: Sandia National Laboratories, Albuquerque, NM, 2016.

[17] C.K. Ho, A review of high-temperature particle receivers for concentrating solar power, Appl. Therm. Eng. 109 (2016) 958–969.

https://doi.org/10.1016/j.applthermaleng.2016.04.103.

[18] C.K. Ho, 6 – A new generation of solid particle and other high-performance receiver designs for concentrating solar thermal (CST) central tower systems, in: Adv. Conc. Sol. Therm. Res. Technol., 2017: pp. 107–128. https://doi.org/10.1016/B978-0-08-100516-3.00006-X.

[19] M.P. Nandakumar, M.S. Thakur, K.S.M.S. Raghavarao, N.P. Ghildyal, Mechanism of solid particle degradation by Aspergillus niger in solid state fermentation, Process Biochem. 29 (1994) 545–551. https://doi.org/10.1016/0032-9592(94)80016-2.

[20] A. Palacios, A. Calderón, C. Barreneche, J. Bertomeu, M. Segarra, A.I. Fernández, Study on solar absorptance and thermal stability of solid particles materials used as TES at high temperature on different aging stages for CSP applications., Energy Mater. Sol. Cells. (2019).

[21] A. Calderón, C. Barreneche, A. Palacios, M. Segarra, C. Prieto, A. Rodriguez-Sanchez, A.I. Fernández, Review of solid particle materials for heat transfer fluid and thermal energy storage in solar thermal power plants., Energy Storage. Under revi (2019).

[22] G.A. Schneider, G. Petzow, Thermal Shock and Thermal Fatigue Behavior of Advanced Ceramics, Springer-Science+Business Media, B.V., Munich, 1992. https://doi.org/10.1007/978-94-015-8200-1.

[23] P.K.K. Panda, T.S.S. Kannan, J. Dubois, C. Olagnon, G. Fantozzi, Thermal shock and thermal fatigue study of ceramic materials on a newly developed ascending thermal shock test equipment, Sci. Technol. Adv. Mater. 3 (2002) 327–334. https://doi.org/10.1016/S1468-6996(02)00029-3.

[24] C. Ho, J. Christian, D. Gill, A. Moya, S. Jeter, S. Abdel-Khalik, D. Sadowski, N. Siegel, H. Al-Ansary, L. Amsbeck, B. Gobereit, R. Buck, Technology Advancements for Next Generation Falling Particle Receivers, Energy Procedia. 49 (2014) 398–407. https://doi.org/10.1016/j.egypro.2014.03.043.

[25] Z. Ma, G. Glatzmaier, M. Mehos, Fluidized Bed Technology for Concentrating Solar Power With Thermal Energy Storage, J. Sol. Energy Eng. 136 (2014) 031014. https://doi.org/10.1115/1.4027262.

[26] G. Flamant, D. Gauthier, H. Benoit, J.-L. Sans, R. Garcia, B. Boissière, R. Ansart, M. Hemati, Dense suspension of solid particles as a new heat transfer fluid for concentrated solar thermal plants: On-sun proof of concept, Chem. Eng. Sci. 102 (2013) 567–576. https://doi.org/10.1016/j.ces.2013.08.051.

[27] C.K. Ho, S.S. Khalsa, N.P. Siegel, Modeling On-Sun Tests of a Prototype Solid Particle

Receiver for Concentrating Solar Power Processes and Storage, in: ASME 2009 3rd Int. Conf. Energy Sustain. Vol. 2, ASME, 2009: pp. 543–550. https://doi.org/10.1115/ES2009-90035.

[28] N. Siegel, M. Gross, C. Ho, T. Phan, J. Yuan, Physical Properties of Solid Particle Thermal Energy Storage Media for Concentrating Solar Power Applications, Energy Procedia. 49 (2014) 1015–1023. https://doi.org/10.1016/j.egypro.2014.03.109.

[29] L.E. Norena, J.-A. Wang, Advanced Catalytic Materials - Photocatalysis and Other Current Trends, InTech, 2016. https://doi.org/10.5772/60491.

[30] Ansys Inc, Ansys Granta Selector 2020, (2020).

[31] Carboceramics, CarboHSP High-density sintered bauxte proppant. Datasheet., 2015.

[32] Panadyne Inc., Black Silicon Carbide Macro Grit, (2018). http://www.panadyne.com/blacksiliconcarbide_tech.html (accessed December 5, 2018).

[33] Engineering ToolBox, Emissivity Coefficients Materials, (2003). https://www.engineeringtoolbox.com/emissivity-coefficients-d_447.html (accessed June 21, 2018).

[34] N. Siegel, M. Gross, R. Coury, The development of direct absorption and storage media for falling particle solar central receivers, J. Sol. Energy Eng. 137 (2015). https://doi.org/10.1115/1.4030069.

[35] Granta Design Limited, CES Selector 2018, (2018).

[36] C.K. Ho, High Temperature Falling Particle Receiver, SunShot CSP Progr. Rev. 2013. (2013). http://energy.gov/sites/prod/files/2014/01/f7/csp_review_meeting_042413_ho.pdf (accessed January 10, 2015).

[37] C.K. Ho, M. Carlson, K.J. Albrecht, Z. Ma, S. Jeter, C.M. Nguyen, Evaluation of Alternative Designs for a High Temperature Particle-to-sCO2 Heat Exchanger, J. Sol. Energy Eng. Trans. ASME. 141 (2019).

[38] K.J. Albrecht, C.K. Ho, Heat Transfer Models of Moving Packed-Bed Particle-to-sCO2 Heat Exchangers, J. Sol. Energy Eng. Trans. ASME. 141 (2019). https://doi.org/10.1115/1.4041546.

[39] M.T. Dunham, B.D. Iverson, High-efficiency thermodynamic power cycles for concentrated solar power systems, Renew. Sustain. Energy Rev. 30 (2014) 758–770. https://doi.org/10.1016/j.rser.2013.11.010.

[40] G. Ferrer, C. Barreneche, A. Solé, I. Martorell, L.F. Cabeza, New proposed methodology for specific heat capacity determination of materials for thermal energy storage (TES) by

DSC, J. Energy Storage. 11 (2017) 1–6. https://doi.org/10.1016/j.est.2017.02.002.

[41] Y. Pan, J.L. Baptista, Chemical instability of silicon carbide in the presence of transition metals, J. Am. Ceram. Soc. 79 (1996) 2017–2026. https://doi.org/10.1111/j.1151-2916.1996.tb08932.x.

[39] N. Siegel, M.D. Gross, R. Coury. The Development of Direct Absorption and Storage Media for Falling Particle Solar Central Receivers. J. of Sol. Energy Eng. 137(4) (2015), 41003-1-7. https://doi.org/10.1115/1.4030069